

## About Cloudiness Low Boundary over Antarctic Peninsula

Irina V. Chernykh, Oleg A. Alduchov,  
*Russian Research Institute of Hydrometeorological Information- Word Data Center, Obninsk, Russia,*  
*E-mails: [civ@meteo.ru](mailto:civ@meteo.ru) , [aoa@meteo.ru](mailto:aoa@meteo.ru)*  
 and Victor E. Lagun,  
*Arctic and Antarctic Research Institute, St. Petersburg, Russia*  
*E-mails: [lagun@aari.nw.ru](mailto:lagun@aari.nw.ru)*

Last time the researches of cloudiness vertical macrostructure and its climatic changes on base sonde observations are conducted in Russia, USA, Great Britain very active [Chernykh et al. 2001, 2003a, Naud, 2003, Wang, 1999]. This can be explained by clouds effect on solar radiation. Antarctic peninsula is a region with good known warming [Comiso, 2000; Marshall et al. 2002]. It is known that low boundary (LB) is one of main characteristics of cloudiness. In this paper mean values of LB for atmospheric layers 0-2 km, 2-6 km, 6-10 km, 0-10 km for different cloud amount 0-20%, 0-60%, 0-80%, 0-100% of the sky are presented for all seasons and for year. Also climatic changes of LB are discussed. Researches was made for Russian station Bellingshausen, placed near Antarctic peninsula, because warming for this station was detected by surface, sonde and satellite observations [Comiso J.C., 2000; Chernykh and Alduchov, 2003b, 2003c].

Researches are made on base Aerological dataset CARDS (Eskridge et al. 1995) for period 1970-1999 years. CE-method was used to determine cloud boundaries and amount from temperature and humidity profiles [Chernykh and Eskridge 1996, Chernykh et al, 2001]. Trends in anomalies for all parameters were calculated by linear regression with using measured values with provision for correlation dependence in time.

Multiyear mean values of LB for cloud layers with cloud amount 0-100% in atmospheric layers 0-2 km, 2-6 km, 6-10 km equal to 488 m, 2794 m and 6850 m accordingly (Table 1). The values vary with season and gradation of cloud amount (0-20%, 0-60%, 0-80% 0-100% of the sky). For some comparison with previous results note, that stratus is most frequently occurring cloud type at region around Bellingshausen for all seasons [Warren et al., 1986]. An example, for winter<sup>1</sup> average base height is 46 decameters for stratus, stratocumulus and fog [Warren et al., 1986]. As it follows from Table 1, for winter mean value of low boundary detected from sonde measurements equal 472 m. It is easy to see, that for winter difference between averaged low boundaries determined from surface observations and detected by CE -method from temperature and humidity profiles for low clouds is near 12 meters. So, agreement enough good. As it was shown before, value of the mistake in determination of cloud boundaries from sonde measurement depends from time constants of humidity and temperature sensors [Chernykh et al, 2001]. But in fact, it depends from time constant of humidity sensors largely, because time constant for temperature sensors is well below than for humidity sensors. According information from AARI, over all period of sonde observations at station Bellingshausen (1970-1999 years) relative humidity was measured by goldbeater's skin hygrometer with time constant of near 0.7 min troposphere.

TABLE 1. Averaged values of low boundary for cloud layers detected by CE-method in atmospheric layers 0-2 km, 2-6 km, 6-10 km and 0-10 km for cloud amount 0-20%, 0-60%, 0-80%, 0-100% of the sky. Seasons: I - December - February; II – March- May; III – June- August; IV – September-November.

Cloud amount	Atmospheric layer 0-2 km					Atmospheric layer 2-6 km				
	Season				Year	Season				Year
	1	2	3	4		1	2	3	4	
0-20%	653	664	883	819	755	3015	2974	2918	3011	2987
0-60%	569	598	688	668	626	2889	2908	2890	2990	2927
0-80%	550	563	688	625	598	2859	2835	2910	2928	2887
0-100%	472	481	504	496	488	2785	2741	2843	2805	2794

Cloud amount	Atmospheric layer 6-10 km					Atmospheric layer 0-10 km				
	Season				Year	Season				Year
	1	2	3	4		1	2	3	4	
0-20%	6813	6791	6628	6704	6771	1708	1245	1600	2452	1747
0-60%	6713	6791	6778	6717	6752	955	924	1353	1177	1145
0-80%	6770	6853	6782	6738	6780	867	837	1379	987	1013
0-100%	6894	6854	6812	6818	6850	732	661	755	726	723

<sup>1</sup> For other seasons base heights for stratus for region around Bellingshausen are absent in Warren et al., 1986

In atmospheric layer 0-10 km multiyear mean value of LB for cloud layers with amount 0-100 % equal to 723 m (Table 1). Together with cloud amount increasing from 0-20% to 0-80% LB mean decrease from 1747 m to 1013 m.

It was founded that low boundaries for clouds with amount 0-100% of the sky in atmospheric layers 0-2 km and 0-10 km for Bellingshausen decrease with decadal changes of  $-35^*$  m/decade and  $-66^*$  m/decade accordingly<sup>2</sup>.

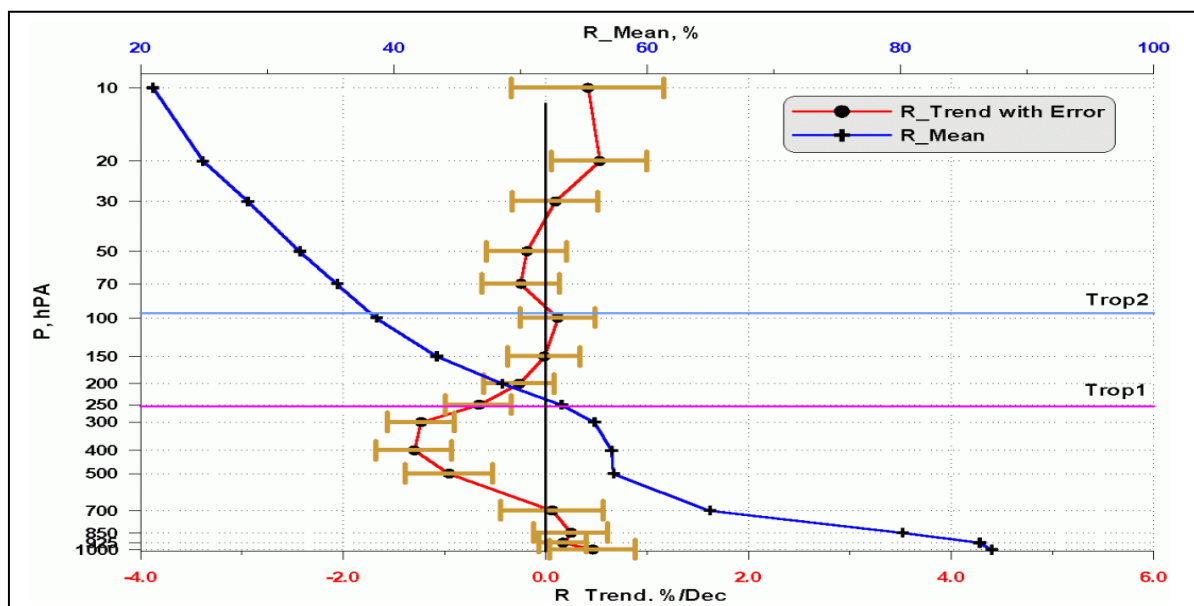


Figure 1. Mean and trends in anomalies of relative humidity R for standard isobaric levels for Bellingshausen. 1970-1999 years. CARDS. Trends in anomalies were calculated by linear regression with using measured values with provision for correlation dependence in time.

This can be partially explained by small increasing of relative humidity in low troposphere, as indicate fig.1. Moreover increasing in frequency of low clouds with decadal changes of  $2.1 \text{ \%decade}^{-1}$  was founded in spring. Note, that largest trend for surface temperature anomalies ( $0.65 \text{ }^\circ\text{C decade}^{-1}$ ) was detected just for spring too (Chernykh and Alduchov, 2003c).

This study is useful to gain insight into climate and climate change in Antarctica. Further researches should be useful. The research was partly supported by RBRF, project 01-05-65285.

## References

- Chernykh I.V., O.A. Alduchov, and R. E. Eskridge, 2001: Trends in low and high cloud boundaries and errors in height determination of cloud boundaries. *Bull. Amer. Meteor. Soc.*, **82**, 1941-1947.
- Chernykh I. V. and R. E. Eskridge, 1996: Determination of cloud amount and level from radiosonde soundings. *J.Appl. Meteorol.*, **35**, 1362-1369.
- Chernykh I.V., O.A. Alduchov, R. E. Eskridge, 2003a: Reply to comments of D.J. Seidel and I. Durre on "Trends in low and high cloud boundaries and Errors in height determination of cloud boundaries". *Bull. of Amer. Met. Society*. Vol. 84, No. 2. P.241-247.
- Chernykh I.V., O.A. Alduchov, 2003b: Analysis of Climatic Changes of Cloud Layers Vertical Structure in Atmospheric Layer below 250 hPa in Antarctica. 27 Annual Climate Diagnostics and Prediction Workshop. 21-25 October 2002. Virginia. USA [http://www.cpc.ncep.noaa.gov/products/outreach/proceedings/cdw27\\_proceedings/ichernykh\\_2002.pdf](http://www.cpc.ncep.noaa.gov/products/outreach/proceedings/cdw27_proceedings/ichernykh_2002.pdf)
- Chernykh I.V., O.A. Alduchov, 2003c: Joint Analysis of Climatic Changes of Surface Temperature and Cloudiness Vertical Structure in Antarctic Region on base CARDS. Research Activities in Atmospheric and Oceanic Modelling. WMO. Recent volume. Climate Change 2001: The Scientific Basis. Contributing of Working Group I to the Third Assessment Report of the Intergovernmental Panel on Climate Change 2001: *Cambridge University Press.*, Cambridge, United Kingdom and New York, NY, USA, 881 p.
- Corniso J.C. , 2000: Variability and trends in Antarctic surface temperatures from in situ and satellite infrared measurements. *J. Climate*, **15**, No 10, 1674-1696.
- Eskridge, R. E., O. A. Alduchov, I. V. Chernykh, P. Zhai, S. R. Doty, and A. C. Polansky, 1995: A Comprehensive Aerological Reference Data Set (CARDS): Rough and systematic errors. *Bull. Amer. Meteor. Soc.*, **76**, 1959-1775.
- Marshall G.J., Lagun V.E., Lachlan-Cope T.A. 2002: Changes in Antarctic Peninsula tropospheric temperatures from 1956-99: a synthesis of observations and reanalysis data // *International Journal of Climatology*. V. 22. P. 291-310.
- Naud C.M., Muller J.P. , E.E. Clothiaux, 2003: Comparison between active sensor and radiosonde cloud boundaries over the ARM Southern Great Plains site. *J. Geophysical research*, Vol. 108, NO. D4, P. 3-1 – 3-12.
- Wang J., Rossow W., T. Uttal and Rozendaal M., 1999: Variability of Cloud Vertical Structure during ASTEX Observed from a Combination of Rawinsonde, Radar, Ceilometer, and Satellite // *Monthly Weather Review*. V. 127. № 10. P. 2484-2502.
- Warren S.G., C.J. Hahn, J. London, R.M. Chervin, R.L. Jenne 1986: Global distribution of total cloud cover and cloud type amount over land. DOE/ER/60085-H1. NCAR/TN-273+STR. NCAR Technical Notes. 222 p.

<sup>2</sup> All trends were detected with significance level not less than 95%.

# Intercomparison of NCEP and ERA reanalyses in terms of characteristics of surface air temperature annual cycle

A.V. Eliseev, M.V. Guseva, I.I. Mokhov and K.G. Rubinstein

A.M. Obukhov Institute of Atmospheric Physics RAS,  
3 Pyzhevsky, 1091017 Moscow, Russia, e-mail: lescha@omega.ifaran.ru

Russian Hydrometcentre, 9, Bol. Predtechensky, 123242 Moscow,  
Russia, e-mail: rubin@mskw.mecom.ru

Climatology and interannual variability of the amplitude-phase characteristics (APC) of the annual cycle (AC) for surface air temperature (SAT) are studied here using the data of NCEP/NCAR [3] and ERA [2] reanalyses for 1958–1998 and 1979–1993 respectively. The APC studied are amplitudes of the annual and semiannual AC harmonics, moments of 0- and  $\pi$ -phases (when SAT equals its annual mean value in spring and autumn, respectively) and interval of exceeding (the period when SAT is higher than its annual mean value) [1]. The two studied reanalyses were compared in terms of the Taylor's diagrams [4] and in terms of the spatial standard deviations.

Table 1 shows the area averaged SAT AC APC for 1979–1993 obtained from the two studied reanalyses together with Taylor's amplitude and spatial correlation coefficients and spatial standard deviation between them. These values are very robust to the particular choice of time intervals to study and change only insignificantly when other intervals are considered. Generally, the two studied reanalyses agree to each other reasonably well. An agreement is better over the Northern Hemisphere in comparison to the Southern Hemisphere. Strong dissimilarities between the reanalyses are found over the polar latitudes (not shown). For 0- and  $\pi$ -phase moments and interval of exceeding the largest deviations are found over the tropics, where these variables are poorly defined. These deviations decrease when only the extratropical areas are considered (Table 1).

Similar (but much wider) intercomparison for atmospheric and climate models is planned nearest future.

This work is partially supported by the Russian Foundation for Basic Research.

## References

- [1] A.V. Eliseev and I.I. Mokhov. Amplitude–phase characteristics of the annual cycle of surface air temperature in the northern hemisphere. *Adv. Atmos. Sci.*, 20(1):1–16, 2003.
- [2] R. Gibson, P. Kallberg, S. Uppala, A. Hernandez, A. Nomura, and E. Serrano. ERA description, ECMWF re-analysis project report series, vol. 1. Technical report, European Centre for Medium-Range Weather Forecasts, Reading, 1997.
- [3] E. Kalnay, M. Kanamitsu, R. Kistler, W. Collins, D. Deaven, L. Gandin, M. Iredell, S. Saha, G. White, J. Woollen, Y. Zhu, A. Leetmaa, R. Reynolds, M. Chelliah, W. Ebisuzaki, W. Higgins, J. Janowiak, K.C. Mo, C. Ropelewski, J. Wang, R. Jenne, and D. Joseph. The NCEP/NCAR 40-year reanalysis project. *Bull. Amer. Met. Soc.*, 77:437–471, 1996.
- [4] T.J. Philips, A. Henderson-Sellers, P. Irannejad, K. McGuffie, H. Zhang, and AMIP2 I Modelling Groups. Validation of land–surface processes in AMIP models: A pilot study. Technical Report PCMDI Rep. 63, Program for Climate Model Diagnosis and Intercomparison, Lawrence Livermore National Laboratory, University of California, Livermore, CA, 2000.

Table 1: SAT AC amplitude–phase characteristics obtained from the data of reanalyses for 1979–1993. The notations are:  $T_{s,1}$  and  $T_{s,2}$  — amplitudes of annual and semiannual SAT harmonics respectively,  $t_s^{(\uparrow)}$  and  $t_s^{(\downarrow)}$  — moments of 0– and  $\pi$ –phases correspondingly,  $t_s^{(+)}$  — interval of exceeding. In every cell upper line shows the climatological value (for  $T_{s,1}$  and  $T_{s,2}$  — in Kelvins, for  $t_s^{(\uparrow)}$  and  $t_s^{(\downarrow)}$  and  $t_s^{(+)}$  — in days since the beginning of the year, for  $t_s^{(+)}$  — in days) from the NCEP and ERA data, respectively (separated by commas). Middle line presents Taylor’s amplitude and spatial correlation coefficient correspondingly. Bottom line shows spatial standard deviations between the two reanalyses data for  $T_{s,1}$  and  $T_{s,2}$  — in Kelvins, for  $t_s^{(\uparrow)}$ ,  $t_s^{(\downarrow)}$  and  $t_s^{(+)}$  — in days).

		$T_{s,1}$	$T_{s,2}$	$t_s^{(\uparrow)}$	$t_s^{(\downarrow)}$	$t_s^{(+)}$
Northern Hemisphere	total	6.9, 7.5	1.0, 1.1	110, 114	270, 273	178, 182
		0.87, 0.98	0.95, 0.82	0.97, 0.69	0.96, 0.90	0.96, 0.77
		1.8	0.5	36	22	13
	land	11.6, 13.1	1.5, 1.8	94, 103	258, 263	180, 186
		0.79, 0.97	0.90, 0.70	0.88, 0.44	0.92, 0.87	1.04, 0.51
		2.9	0.7	50	24	17
ocean	4.0, 4.0	0.7, 0.7	120, 121	278, 278	176, 179	
	1.05, 0.99	1.29, 0.85	1.01, 0.85	0.97, 0.92	0.94, 0.89	
	0.6	0.4	23	21	9	
Southern Hemisphere	total	3.6, 3.3	0.9, 0.8	288, 288	126, 128	179, 182
		1.19, 0.93	1.29, 0.96	1.02, 0.93	1.16, 0.78	1.07, 0.73
		1.6	0.5	26	23	13
	land	7.0, 7.1	2.2, 2.1	247, 250	104, 106	172, 182
		0.79, 0.97	0.90, 0.70	0.88, 0.44	0.92, 0.87	1.04, 0.51
		1.8	0.7	33	50	29
ocean	2.8, 2.5	0.5, 0.5	284, 284	131, 133	181, 182	
	1.77, 0.94	1.98, 0.94	1.03, 0.95	1.01, 0.90	1.04, 0.90	
	1.6	0.4	24	10	6	
Northern extratropics (30–90N)	total	11.3, 12.4	1.4, 1.5	110, 111	285, 289	175, 178
		0.82, 0.96	1.01, 0.71	0.98, 0.97	1.17, 0.95	0.91, 0.86
		2.5	0.7	5	6	7
	land	15.2, 17.6	1.7, 1.9	94, 95	273, 279	179, 184
		0.71, 0.93	0.98, 0.62	0.80, 0.73	1.10, 0.68	0.93, 0.71
		3.4	0.7	6	8	9
ocean	7.5, 7.3	1.2, 1.1	125, 126	296, 298	171, 173	
	1.07, 0.99	1.32, 0.77	0.94, 0.98	1.22, 0.96	0.92, 0.91	
	0.9	0.6	4	5	5	
Southern extratropics (30–90S)	total	5.1, 4.5	1.3, 1.0	302, 302	114, 115	177, 178
		1.20, 0.92	1.29, 0.96	1.04, 0.95	1.14, 0.97	1.16, 0.95
		2.2	0.7	5	6	5
	land	13.0, 13.0	4.3, 3.7	275, 278	70, 76	161, 163
		1.11, 0.90	1.26, 0.96	0.75, 0.47	1.33, 0.88	1.22, 0.95
		2.2	1.1	7	10	7
ocean	3.9, 3.1	0.8, 0.6	306, 305	122, 122	180, 180	
	1.92, 0.94	2.03, 0.95	0.97, 0.93	1.14, 0.95	1.16, 0.94	
	2.2	0.6	5	5	5	

# WGNE assessment of Quantitative Precipitation Forecasts from Operational Numerical Weather Prediction Models over the U.K.

M. Goeber\*, C.A. Wilson  
Met Office, London Road, Bracknell, RG12 2SZ, U.K.

Up to 3-day forecasts of daily precipitation accumulation from the 12 UTC run of 7 global, operational numerical weather prediction models as well as the mean and median forecast of those models were verified over the U.K. for more than two years (different samples between models because of transmission problems etc.). The model data were up/down-scaled by box-averaging to a common resolution of  $96 * 96 km^2$ . The forecasts were compared against upscaled daily accumulations derived from quality controlled and corrected radar observations (Harrison *et al* (2000)) comprising the British Isles and adjacent waters.

Marginal, joint and conditional (denoted by a bar '|') probabilities  $p$  of events in certain categories were computed on the basis of monthly and total contingency tables, respectively. Plots are presented of the frequency bias  $FB$ , odds ratio  $\theta$  and likelihood ratios  $L$  according to the following definitions (Stephenson (2000), Göber *et al* (2003)):

$$FB = \frac{p(f)}{p(o)}; \quad L(rain) = \frac{p(o|f)}{p(\bar{o}|f)}; \quad L(no - rain) = \frac{p(\bar{o}|\bar{f})}{p(o|\bar{f})}; \quad \theta = L(rain) * L(no - rain)$$

where  $f$  ( $o$ ) denotes the forecast (observed) event and  $\bar{f}$  ( $\bar{o}$ ) denotes the not forecast (not observed) event.

Fig. 1 shows that most models are reasonably well calibrated, with the MEAN and MEDIAN (MM) forecasts showing the behavior expected from a smoothed forecast. The skill of the forecasts ( $\log \theta$ ) increases slightly with accumulation. The main cause of this is the stronger drop in false alarm rate  $p(\bar{o}|f)$  than the drop in hit rate  $p(o|f)$  with threshold (not shown). Note, that the odds ratio corrects for the 'base-rate' effect, which is a strong influence in other scores like Equitable Threat Score, i.e. it accounts for the fact that for *rare* events one can not get lots of hits and there are lots of potential cases to issue a false alarm (Göber *et al* (2003)). The MM forecasts are generally better than the best single model. A split of the odds ratio into forecasts of the event and non-event reveals that the MM forecasts are good in both categories whereas single models are good in either forecasting the event or the non-event. Figs. 2 of the time evolution of the monthly scores show a substantial variability of the monthly performance of the models themselves and between the models. Again, the MM forecasts perform relatively well in most months.

## References

- Göber, M, C. A. Wilson, S. F. Milton, and D. B. Stephenson, 2003: Fairplay in the verification of operational quantitative precipitation forecasts. *J. Hydrol.*, *submitted for publication*.
- Harrison, D. L., S. J. Driscoll, and M. Kitchen, 2000: Improving precipitation estimates from weather radar using quality control and correction techniques. *Meteorol. Appl.*, **6**, 135–144.
- Stephenson, D. B., 2000: Use of the 'odds ratio' for diagnosing forecast skill. *Wea. Forecasting*, **15**, 221–232.

---

\* © Controller, Her Majesty's Stationery Office, Norwich, England, 2003; email: martin.goeber@metoffice.com

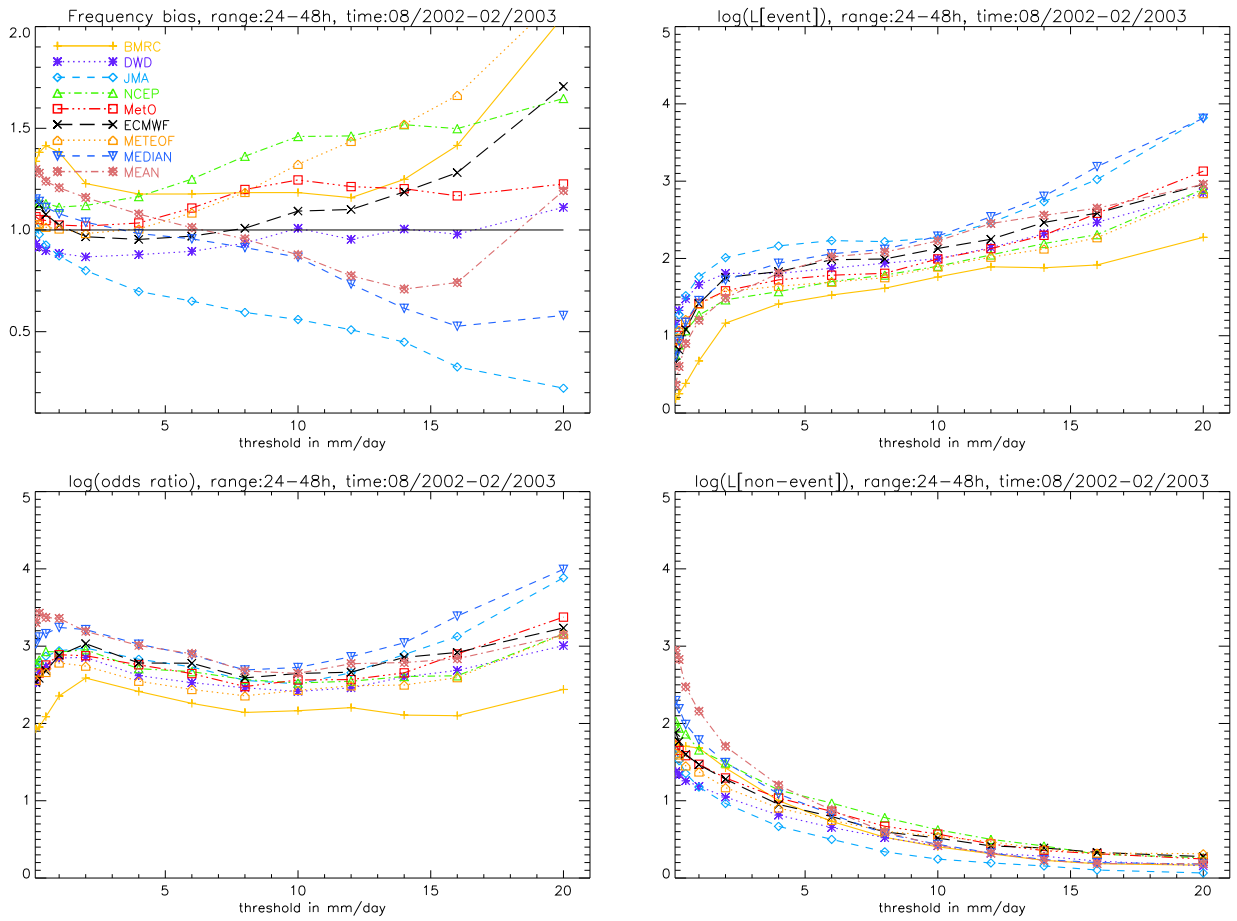


Figure 1: Frequency bias  $FB$  (upper left), odds ratio  $\ln\theta$  (lower left) and its split into the likelihood ratios  $L(\text{rain})$ ,  $L(\text{no-rain})$  (upper and lower right column) as a function of precipitation threshold for daily accumulations 2 days into the 12-UTC forecasts based on a sample from 08/02-02/03. Mean and Median are taken from all models available at a particular grid box and time.

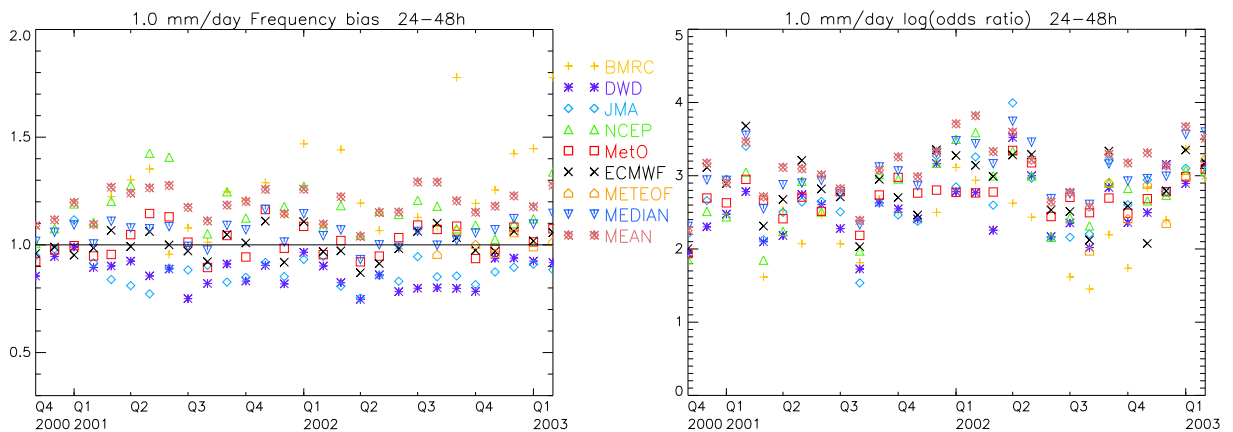


Figure 2: Monthly time series of frequency bias (left) and  $\log(\text{odds ratio})$  (right) for daily accumulations of more than 1.0 mm/day of day two of the 12-UTC forecasts. Note missing data and the longer time interval than Fig. 1.

## Global cloudiness: Tendencies of change from ISCCP data

I.I. Mokhov<sup>1</sup> and A.V. Chernokulsky<sup>1,2</sup>

<sup>1</sup>Institute of Atmospheric Physics RAS, Moscow, Russia

<sup>2</sup>Moscow State University, Russia

mokhov@omega.ifaran.ru

One of the important but as yet unsolved problems in climate research is the effect of clouds on radiation and temperature conditions as well as the dependence of clouds on temperature and circulation conditions (Houghton et al., 2001). Due to the treatment of clouds and cloud feedback effects in climate models there is a significant uncertainty about the sensitivity of the climate system to anthropogenic forcing (Mokhov, 1981; Schlesinger and Mitchell, 1986; Houghton et al., 2001). There is uncertainty even in the sign of changes in cloudiness accompanying global temperature changes (global warming, in particular) from observations and simulations (Mokhov, 1985; Henderson-Sellers, 1986; Mokhov, 1991a,b; Mokhov and Love, 1995; Rossow and Schiffer, 1999; Houghton et al., 2001).

We present here some estimates of the global scale relationship between cloudiness from ISCCP data (Rossow and Schiffer, 1999) and surface air temperature from (Jones, 1999) for the Northern (NH) and Southern (SH) Hemispheres. Table 1 shows the results of linear regressions (coefficients of regression with their standard deviations in brackets and coefficients of correlation) of the total cloud amount to the global or hemispheric surface air temperature by annual-mean data for the period 1984-1999. Coefficients of regressions in Table 1 characterize the temperature sensitivity of global and hemispheric cloudiness and also for different latitudinal belts.

Table 1.

Cloudiness : surface air temperature		Regression coefficient, K <sup>-1</sup>	Correlation coefficient
With polar latitudes	Global	-0.031 (±0.013)	-0.55
	NH	-0.034 (±0.012)	-0.61
	SH	-0.009 (±0.018)	-0.13
Without polar latitudes (<60°)	NH+SH	-0.052 (±0.018)	-0.63
	NH	-0.045 (±0.014)	-0.66
	SH	-0.041 (±0.029)	-0.36
Tropical latitudes (<30°)	NH+SH	-0.076 (±0.024)	-0.65
	NH	-0.063 (±0.019)	-0.67
	SH	-0.056 (±0.042)	-0.34
Middle latitudes (60°-30°)	NH	-0.027 (±0.011)	-0.56
	SH	-0.021 (±0.016)	-0.33

Figure 1 illustrates the appropriate linear regressions of the NH tropical and extrapolar cloudiness to the NH surface air temperature.

Negative correlation of cloudiness and temperature characterizes the appropriate relationship as a positive climate feedback.

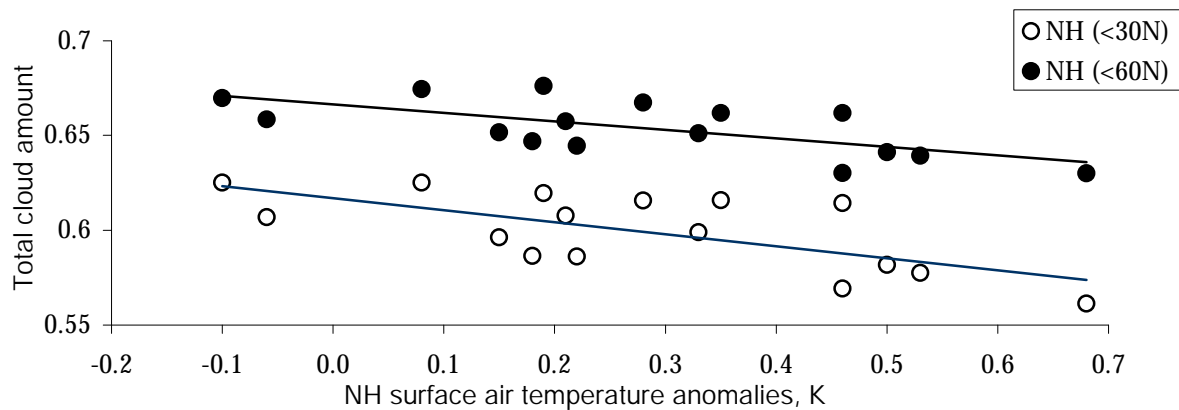


Fig. 1

This work was partly supported by the Russian Foundation for Basic Research.

### References

- Henderson-Sellers, A., 1986: Increasing cloud in a warmer world. *Clim. Change*, 9, 267-309.
- Houghton, J.T., et al. (editors), 2001: *Climate Change 2001: The Scientific Basis. Contribution of Working Group I to the Third Assessment Report of the Intergovernmental Panel on Climate Change*. Cambridge Univ. Press, Cambridge, 881 pp.
- Jones P.D., New M., Parker D.E. et al. Surface air temperature and its changes over the past 150 years // *Rev. Geophys.* 1999. V.37. P.173-199.
- Mokhov, I. I., 1981: Effect of CO<sub>2</sub> on the thermal regime of the Earth's climatic system, *Sov. Meteorol. Hydrol.*, 4, 17-26.
- Mokhov, I.I., 1985: Global relationship between cloudiness and temperature as revealed by data on their interannual variability, *Izvestiya, Atmos. Oceanic Phys.*, 21, 700-704.
- Mokhov, I.I., 1991: Global Cloudiness: Tendencies of change. ISPP-7 "Piero Caldirola", Controlled Active Global Experiments (CAGE). E. Sindoni and A.Y. Wong (Eds.), Societa Italiana di Fisica, Bologna, 19-37.
- Mokhov, I.I., 1991: Trends in global and polar cloudiness from satellite data. *Proc. Intern.Conf. on the Role of the Polar Regions in Global Change. Vol. I*. G. Weller, C.L. Wilson and B.A.B. Severin (Eds.). GIUAF/ CGCASR Univ. of Alaska Fairbanks, Fairbanks, 176-182.
- Mokhov I.I., Schlesinger M.E. Analysis of global cloudiness. 2. Comparison of ground-based and satellite-based cloud climatologies. *J. Geophys. Res.*, 1994, 99D, 17045-17065.
- Mokhov, I.I., and P.K. Love, 1995: Diagnostics of cloudiness evolution in the annual cycle and interannual variability in the AMIP (Cloudiness Diagnostics Subproject 13). *Proc. First Int. AMIP Sci. Conf.*, Monterrey, CA, U.S. Department of Energy and World Climate Programme, WMO/TD-752, 49-53.
- Rossow, W.B., and R.A. Schiffer, 1999: Advances in understanding clouds from ISCCP. *Bull. Amer. Meteor. Soc.*, 80(11), 2261-2287.
- Schlesinger, M.E., and J.F.B. Mitchell, 1986: Model projections of the equilibrium climate response to increased carbon dioxide. *Projecting the Climatic Effects of Increasing Carbon Dioxide*, M.C. MacCracken and F.M. Luther, Eds., U.S. Department of Energy, Washington, D.C., 81-147.

# Intense Arctic and Antarctic mesocyclones (polar lows) and their variability

I.I. Mokhov<sup>1</sup> and M.G. Akperov<sup>2</sup>

<sup>1</sup>Institute of Atmospheric Physics, Moscow, Russia

<sup>2</sup>Moscow State University, Russia

mokhov@omega.ifaran.ru

Some characteristics of intense polar mesocyclones or polar lows (PL) and of their variations are presented. In particular, comma- and spiral-type PLs in the North-European Arctic basin (between 20°W and 70°E) during 1981-1995 and over the Southern Ocean basin (between 0°E and 90°E) near Antarctic during 1984-1995 (Lagun and Lutsenko, 2000) are analyzed (see also Mokhov and Priputnev, 2001). The total number of analyzed PLs was 253 in the Arctic basin and 834 in the Antarctic basin.

Frequency of spiral- and comma-types of PLs is the lowest one in summer. PLs are the most frequent in winter and also in spring. There are also remarkable interannual variations of the PL frequency with a period about 5-6 years and correlation (particularly for comma-type) for Arctic (with a lag) and Antarctic basins.

Figure 1 shows annual-mean number of days with comma- and spiral-type cyclones and their total number in dependence on the PLs size (diameter) for the period 1981-1995 (a) and also for comma-types during different 5-year periods (b) in the North-European Arctic basin.

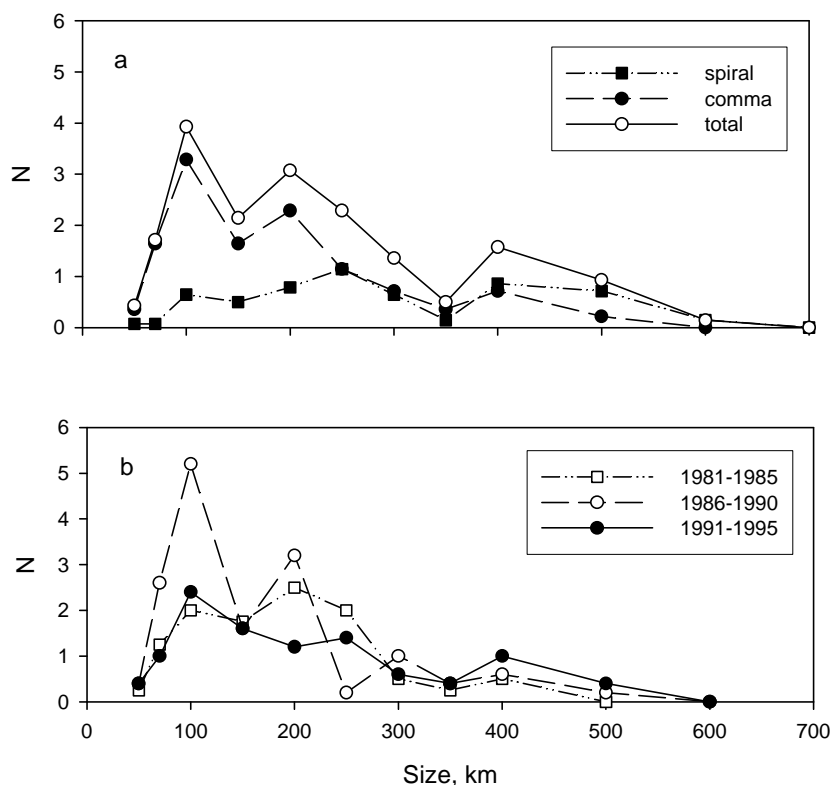


Fig.1.

Probability density functions (PDF) of the annual-mean PL number in the North-European Arctic basin in dependence of the PL size show several extremes. Local PDF maxima during the total period 1981-1995 and for different 5-year periods are displayed at PL

sizes about 400, 200-250 and 100 km. It should be noted that PDFs for comma-types and spiral-types are very different.

Figure 2 shows annual-mean number of days with comma- and spiral-type cyclones and their total number in dependence on the PLs size for the period 1984-1995 (a) and also for comma-types during different 5-year periods (b) in the Southern Ocean basin.

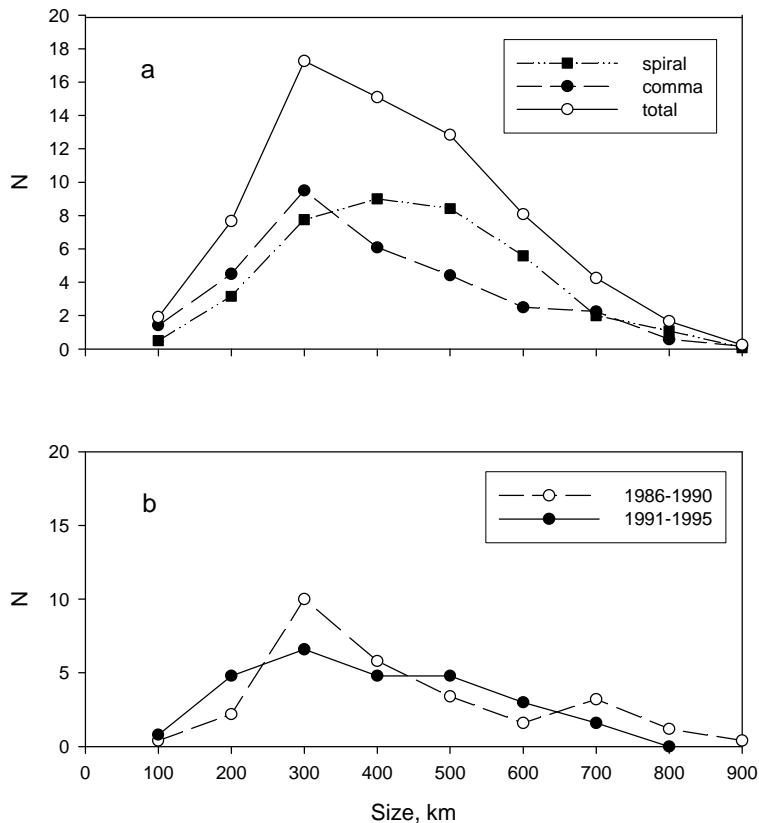


Fig.2.

The PDFs for PLs in dependence on their size over the Antarctic basin display only one maximum (about 300 km for comma-type and about 400 km for spiral-type) for the total period 1984-1995 (Fig.2a) with some peculiarities for different 5-year periods (Fig.2b). In comparison with Arctic mesocyclones the Antarctic ones are remarkably larger - up to 800 km and even larger. In the Arctic basin no PLs have been noted larger than 600 km.

Different features in PDFs for the Arctic and Antarctic PLs are related with differences of ocean-land distribution, mean seasonal regimes and different mechanisms of the PLs formation and evolution. In particular they can be related with different contribution of baroclinic instability and convection processes. The exhibition of some peculiarities in PDFs depends on statistics (number of analyzed PLs, in particular for short 5-year periods).

This work has been partly supported by the Russian Foundation for Basic Research.

## References

1. Lagun V.E., Lutsenko E.I. Diagnostic study of the polar low genesis event climatology over Arctic and Antarctic seas // EGS XXV General Assembly. Abstracts. Nice, France. 2000.
2. Mokhov I.I., Priputnev S.G. Distribution functions of polar lows depending on size // Research Activities in Atmospheric and Oceanic Modelling. Ed. by H. Ritchie. WMO/TD-No.1064. 2001. P.2.22-2.23.

# Preliminary Experiments for Japanese 25-year Reanalysis Project

Kazutoshi Onogi<sup>1</sup>, Hiroshi Koide<sup>1</sup>, Masami Sakamoto<sup>1</sup>, Nobutaka Mannoji<sup>1</sup>, Nobuo Yamazaki<sup>2</sup>,  
Hirohisa Kamahori<sup>2</sup>, Kiyotoshi Takahashi<sup>2</sup>, Jun'ichi Tsutsui<sup>3</sup>, Hiroaki Hatsushika<sup>3</sup>

<sup>1</sup>Climate Prediction Division/Japan Meteorological Agency, Tokyo, Japan

<sup>2</sup>Meteorological Research Institute/Japan Meteorological Agency, Tsukuba, Japan

<sup>3</sup>Central Research Institute of Electric Power Industry, Abiko, Japan

konogi@naps.kishou.go.jp, hkoide@naps.kishou.go.jp, masami.sakamoto-a@met.kishou.go.jp,  
nmannoji@npd.kishou.go.jp, nyamazak@mri-jma.go.jp, hkamahor@mri-jma.go.jp, ktakahas@mri-jma.go.jp,  
tsutsui@criepi.denken.or.jp, hatsusika@criepi.denken.or.jp

## **1. Introduction**

Japan Meteorological Agency (JMA) and Central Research Institute of Electric Power Industry (CRIEPI) made a contract to conduct a reanalysis as a cooperative research project denominated as JRA-25 (Japanese 25-year Reanalysis Project). The target years of the reanalysis are from 1979 to 2004. JMA and CRIEPI agreed to offer their technical experts, software and computational resources. The period of the contract is for the fiscal years from 2001 to 2005. Reanalysis production will be started late 2003.

## **2. Observational data and Numerical models**

### **1) Observational data**

Conventional data, Atmospheric Motion Vector (AMV) wind data by geostationally satellites and TOVS, SSM/I data by polar orbital satellites will be assimilated in JMA operational model. Data sources are JMA archives and ERA-40 observational data used in ERA-40, which includes the data used in NCEP/NCAR reanalysis. Historical position data of tropical cyclones (TC) and retrieved wind data surrounding TCs were provided by Dr. Fiorino (LLNL/PCMDI). The latter are assimilated to express TCs accurately. GMS AMV data reprocessed by Meteorological Satellite Center (MSC/JMA) from April 1987 onward are assimilated as well.

### **2) Numerical Models**

JMA operational 3DVAR global assimilation system will be used in JRA-25. TOVS 1d data are assimilated in the system. The forecast model for JRA-25 is T106-L40 global model with the top level at 0.4hPa based on the current operational T213-L40 model. For land surface processes, JMA operational SiB scheme is driven by atmospheric forcing parameters. Snow depth analysis is operated once a day using surface snow data. COBE (Centennial in-situ-Observation-Based Estimate of variability of SST and marine meteorological variables) SST data set, which is produced by CPD/JMA by assimilating historical marine observations and covers whole period of JRA-25, will be used.

## **3. Preliminary experiments**

We have made some experiments to investigate impacts of observational data and schemes to be used in JRA-25 before starting production.

### **1) Impact of the TC retrieval wind data**

An experiment is performed to investigate impacts of TC retrieval wind data. Figure 1 shows analysis fields with(top)/without(bottom) the retrieval wind data for North-Western and North-Eastern Pacific Ocean respectively at 18UTC 15th September 1990 during SPECTRUM period. Although TCs are not analyzed in NE Pacific and poorly analyzed in NW Pacific without the retrieval wind data, they are analyzed correctly at their reported position with the retrieval data.

### **2) Land surface processes and Snow analysis**

An experimental data assimilation cycle was executed over 8 month from 1st October 1988. Time series of analyzed snow coverage over Eurasia and North America continents are shown in Figure 2. Snow coverage change naturally during the winter and spring for each continent.

### **3) Quality of reprocessed GMS AMV data**

Quality of reprocessed GMS AMV data were investigated. A Quality Indicator (QI) is attached on each AMV datum. The data are categorized by QI and compared with first guess fields. The first guess fields were created without using the reprocessed AMV data. Data of high quality (QI $\geq$ 85%) have good consistency with first guess field (Figure 3) and few data are rejected by quality controls.

Other experiments will be made further before starting production of JRA-25.

## **Reference and Acknowledgement**

Details of JRA-25 can be referred from <http://www.jreap.org/indexe.html>. We express special thanks to ECMWF and other organizations and individuals who provided observational data.

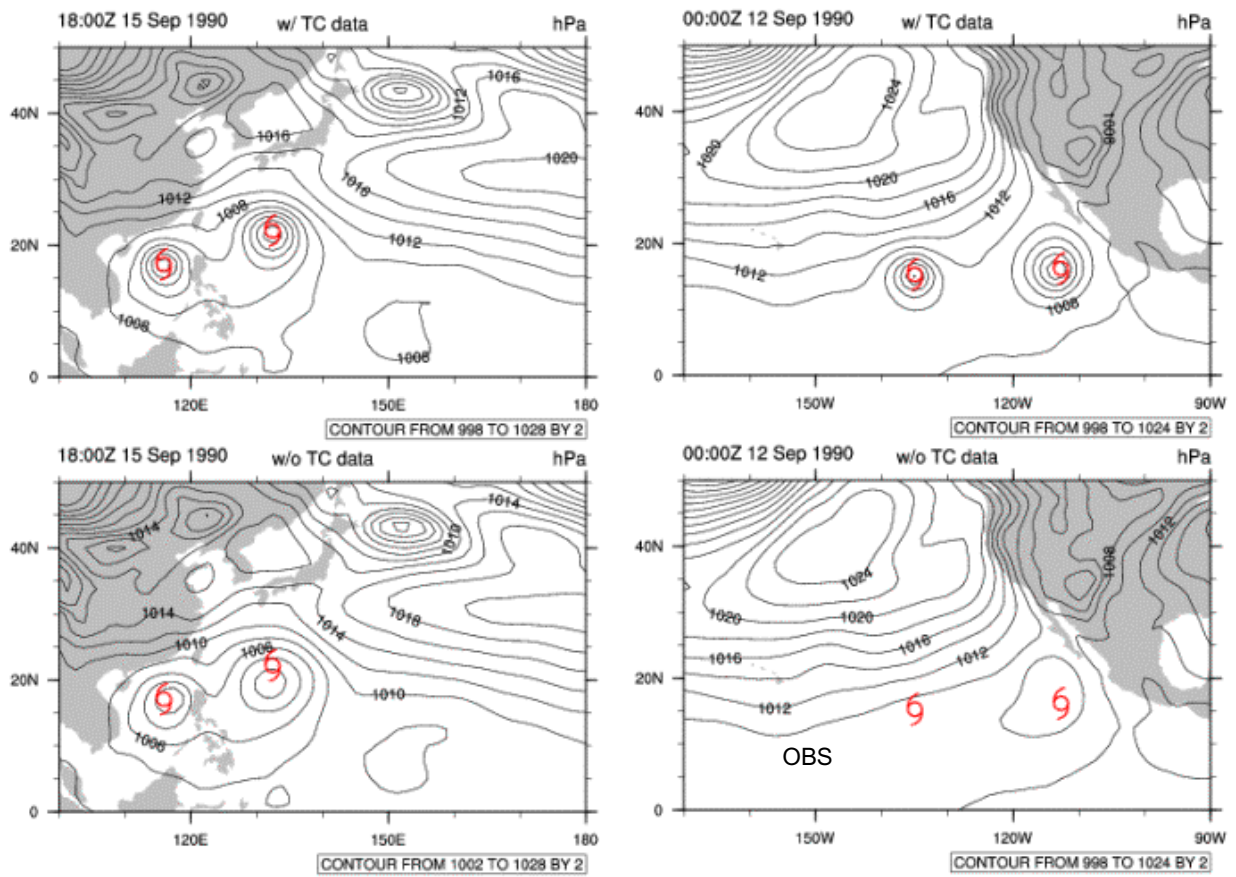


Figure 1 MSLP analysis field of North-Western (left) and North-Eastern (right) Pacific with (top) / without (bottom) TC wind retrieval data.

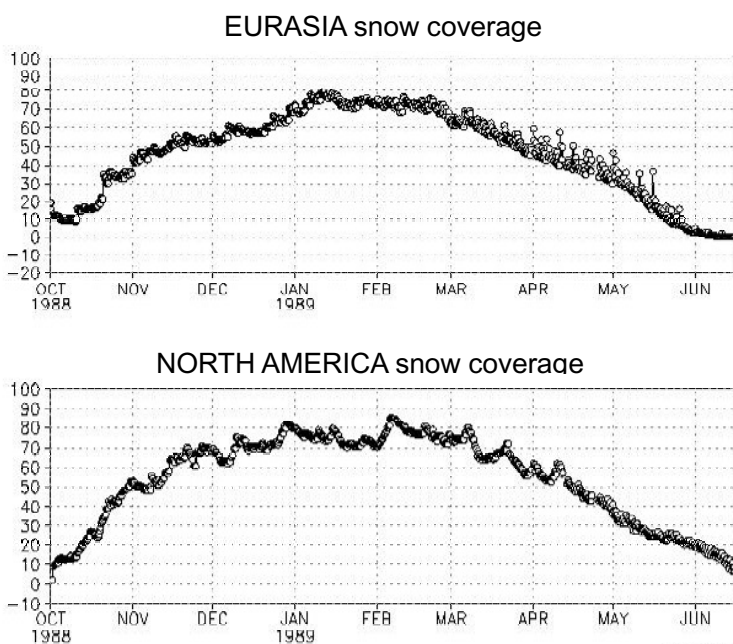


Figure 2 Time series of snow coverage of Eurasia (top) and North America (bottom) continent from 1988.10 to 1989.6

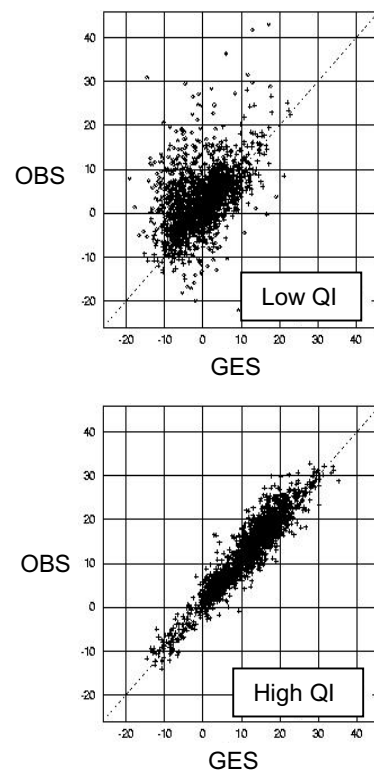


Figure 3 Scatter diagrams of reprocessed GMS AMV data (Low level U-comp. wind) for low QI data (top) and high QI data (bottom)

STATISTICAL MODELS FOR OPERATIVE FORECAST OF  
DANGEROUS CONVECTIVE PHENOMENA LIKE RAINFALLS,  
SQUALLS AND TORNADOES IN THE EUROPEAN PART OF  
RUSSIA AND IN EUROPE

E.V.Perekhodtseva

( *Hydrometeorological Center of Russia, B.Predtechenskii 9-13,  
123242, Moscow, Russia, e-mail: perekhodtseva@rhmc.mecom.ru*)

Development of successful method for automated statistical forecast of heavy rainfalls, as well as strong summer winds, including squalls and tornadoes, that often result in human and material losses, could allow one to take proper measures against destruction of buildings and to protect people. Well-in-advance forecast (from 12 hours to two days) of heavy rainfalls makes possible to take proper measures against floods and to reduce the losses. Prediction of the phenomena involved is a very difficult problem for synoptic till recently. The existing graphic and calculation methods still depend on subjective decision of an operator.

At the present time in Russia there is no hydrodynamic model for forecast of heavy rainfalls and the maximal speed of wind, hence the main tools of objective forecast are statistical methods using the dependence of the phenomena involved on a number of atmospheric parameters (predictors).

Successful development of hydrodynamic models for short- and mid-term forecast and improvement of two-three-day forecasts of pressure, temperature and others parameters allow us to use the prognostic fields of those models for calculations of the discriminant functions in the nodes and the values of probabilities of dangerous precipitation and winds and thus to get fully automated forecasts. Statistical decisive rules for the alternative and probability forecasts for each of the phenomena involved were obtained in accordance with the concept of "perfect prognosis" using the data of objective analysis. For this purpose the teaching samples were automatically arranged that include the values of forty physically substantiated potential predictors.

Then the empirical statistical method was used that involved diagonalization of the mean correlation matrix of the predictors and extraction of diagonal blocks of strongly correlated predictors. Thus for each phenomena the most informative predictors were selected without losing information, those predictors being either a representative of each block or an independent informative predictors. The statistical decisive rules for diagnosis and prognosis of the phenomena involved were calculated for the most informative vector-predictor that includes the most informative (we used the criterion of distance of Mahalanobis and criterion of minimum of entropy by Vapnik-Chervonenkis) and slightly dependent predictors.

For prognosis of the phenomena involved with the given advance period the values of the discriminant functions and the probabilities of the phenomena were calculated using the prognostic values of the hemispherical model in the nodes of the rectangular mesh 150x150 km over the European part of Russia and Europe. In order to change to the alternative forecast the author proposes the empirical threshold values specified for each phenomena and advance period.

According to the Pirsey-Obukhov criterion (T), the success of the 24-hour forecast and the method of forecast of dangerous precipitation in the warm season for the first and second day, as used in Hydrometeorological Center of Russia since 1998 as the main calculation method, is  $T=0,49-068$ . The same is true for the forecast of dangerous squalls and tornadoes, that was tested by Hydrometeorological Center of Russia in 1999-2000 and was included into the automatic prognosis system in the summer of 2001. The method for forecast of very dangerous precipitation (the quantity over 50 mm/12h ) was tested successful in some regions of European part of Russia in 1998-2002 .

The forecast of strong summer wind with the value of velocity over 25m/s is developed for next day and next night to 36 hours ahead and is included into operative system of Hydrometeorological Center of Russia. Nowadays this forecast is produced two times per day as the help tool for a synoptic.

# Optimal nonmodal growth as a contributing cause to the Southern Hemisphere annular mode variability

*Harun Rashid and Ian Simmonds*

School of Earth Sciences, The University of Melbourne Melbourne, Victoria 3010, Australia  
E-mail: harun@earthsci.unimelb.edu.au

The southern annular mode (SAM) is the leading mode of Southern Hemisphere (SH) circulation variability, the temporal evolution of which is characterized by large amplitudes and long persistence. Its spatial structure is dominated by a zonally-symmetric pattern, a see-saw meridional variation of zonal flow anomalies between 40°S and 60°S, and an equivalent barotropic structure in the vertical (e.g., Limpasuvan and Hartmann, 2000; Thompson and Wallace, 2000). Previous investigators have suggested a positive feedback mechanism that explains some of this low-frequency variance (Lorenz and Hartmann, 2001). Here, we propose another mechanism, involving transient nonmodal growths of the anomalies, that is at least as effective as the positive feedback mechanism in increasing the low-frequency variance of the SAM.

Using the *vector autoregressive modeling* (VAR) technique, we first derive a number of empirical models of SAM variability from a 22-year (1979–2000) record of NCEP/DOE Reanalysis 2. These models are then analyzed applying the ideas of the generalized stability theory (Farrell and Ioannou, 1996). Two VAR models, of order 1 and 3, are investigated in detail. The system matrices characterizing these models are found to be *nonnormal* (i.e., they do not commute with their respective transposes), indicating that these matrices have *nonorthogonal* sets of eigenvectors. Using a Schur decomposition, the system matrix  $\mathbf{R}$  was separated into a normal matrix  $\mathbf{N}$  and an asymmetric matrix  $\mathbf{A}$ , which is related to the *departure from normality* of  $\mathbf{R}$  (Golub and Loan, 1996). An examination of the elements of  $\mathbf{A}$  shows that the main source of nonnormality of  $\mathbf{R}$  is the strong forcing of the SAM provided by the high-frequency eddies (of periods 2–8 days). The above Schur decomposition also enabled us to determine the relative importance of the effects of nonnormality and of the positive feedback on SAM variability. This was done in two stages. First, SAM indexes were simulated using, in turn, the full coefficient matrix  $\mathbf{R}$  the normal matrix  $\mathbf{N}$ , and the matrix  $\mathbf{R}$  with the element representing the zonal-wind feedback on the eddies set to zero. Then, the power spectra of the simulated SAM indexes were computed, which are displayed in Fig. 1. In each case, white-noise realizations having the same noise covariance matrix were used for driving the simulated processes. Therefore, the differences between the three spectra in Fig. 1 are solely due to the differences in deterministic contributions caused by the presence/absence of nonnormality and of feedback. The figure shows that both the nonnormality and the zonal-wind feedback have significant effects on the low-frequency variance of the SAM, with the former having a larger overall effect.

Because of the nonnormality of the system matrix  $\mathbf{R}$ , the anomalies governed by this system may undergo *transient growths* due to modal interferences (Farrell and Ioannou, 1996), even though the system under consideration is stable. The *optimal* transient growth in such a system is associated with the right singular vector ( $V_1$ ) corresponding to the largest singular value ( $\sigma_1$ ) of  $\mathbf{R}$ . If  $\sigma_1 > 1$ , then an initial field of anomalies projecting strongly on  $V_1$  should experience optimal nonmodal growth before its ultimate decay. To determine whether this nonmodal growth can be detected in the temporal evolution of the observed SAM index, we constructed composites of the time-lagged SAM index corresponding to initial fields that project strongly on  $V_1$ , for the VAR(1) and VAR(3) models. The composites are presented in Fig. 2 separately for the positive anomaly growths and negative anomaly growths. The figure shows that the anomaly fields that have a significant projection on  $V_1$  are indeed followed by the evolutions of the SAM index with growths of positive or negative anomalies. This result combined with

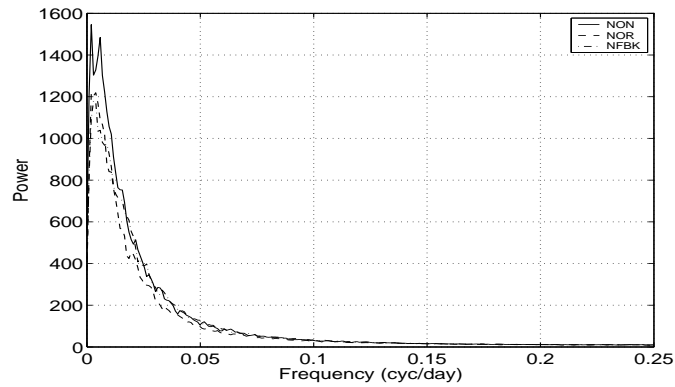


Figure 1: Power spectra of the simulated SAM indexes showing the effects of nonnormality and feedback on the SAM variability in the VAR(1) model.

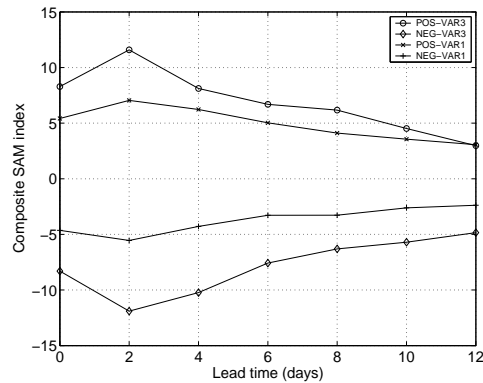


Figure 2: Composites of the time-lagged SAM index corresponding to initial perturbations that project strongly on the optimal perturbations of the VAR(1) and VAR(3) models.

that presented in Fig 1 show that a considerable fraction of the low-frequency variance of the SAM is caused by optimal nonmodal growths of the anomalies.

## References

- Farrell, B. F. and P. J. Ioannou: 1996, Generalized stability theory. Part 1: Autonomous operators. *J. Atmos. Sci.*, **53**, 2025–2040.
- Golub, G. H. and C. F. V. Loan: 1996, *Matrix Computations. 3rd ed.* The Johns Hopkins University Press, Baltimore and London, 694 pp.
- Limpasuvan, V. and D. L. Hartmann: 2000, Wave-maintained annular modes of climate variability. *J. Climate*, **13**, 4414–4429.
- Lorenz, D. J. and D. L. Hartmann: 2001, Eddy–zonal flow feedback in the Southern Hemisphere. *J. Atmos. Sci.*, **58**, 3312–3327.
- Thompson, D. W. J. and J. M. Wallace: 2000, Annular modes in the extratropical circulation. Part I: Month-to-month variability. *J. Climate*, **13**, 1000–1016.

## Deutscher Wetterdienst (DWD) meteorological data set for the development of a flood forecasting system

Gdaly Rivin, Erdmann Heise

Deutscher Wetterdienst, Research and Development, 63067 Offenbach, Germany  
<http://www.dwd.de>, [Gdaly.Rivin@dwd.de](mailto:Gdaly.Rivin@dwd.de), [Erdmann.Heise@dwd.de](mailto:Erdmann.Heise@dwd.de)

The development of a European flood forecasting system for early flood warning up to 10 days in advance [1,2] on the basis of the ensemble prediction system of the European Centre for Medium Range Weather Forecasts (ECMWF) is supported by examining historical flood periods. In co-operation with ECMWF and with the Danish Meteorological Institute, DWD prepared data sets which include all meteorological fields necessary as input fields to hydrological models. Four flood cases in different European river basins for different seasons (autumn, winter and summer) were investigated: a) Po – 1994, November, b) Rhine, Meuse – 1995, January, c) Odra – 1997, July, d) Elbe — 2002, August.

The fields are based on the analysis of observed precipitation and on model forecasts:

- 48 h forecasts by DWD's limited area model LM [3] (ca. 7 km resolution, model area is Central Europe, data provided at hourly intervals);
- 156 h forecasts by DWD's global model GME [4] (model resolution ca. 60 km, data provided at 6 hourly intervals on a  $0.75^\circ \times 0.75^\circ$  grid with NW-corner at  $75^\circ$  N,  $35^\circ$  W and SE-corner at  $30^\circ$  N,  $45^\circ$  E);
- analyses of 24 h precipitation observations for the LM area in ca. 7 km resolution.

In Figure 1 results are shown for the region of the Alps and of Northern Italy. The analyses of the observed precipitation distribution for November 05, 1994, 06 UTC to November 06, 1994, 06 UTC are based on the routinely distributed measurements of Synoptic stations (631 observations in this case, Figure 1a), and on the same stations but additionally observations collected during the Mesoscale Alpine Programme (631 + 5173 observations, Figure 1b), respectively. For comparison, a 18 to 42 hours forecast by LM is given (Figure 1c), which started at November 04, 1994, 12 UTC. From this figure we can conclude that a) the use of high resolution precipitation data provides analyses significantly different from analyses based on Synoptic data only, b) LM gives a very good indication of tremendous rainfall in the eastern part of the Alpine arc, and c) LM overpredicts the amount of precipitation in this case.

**Acknowledgement:** This work was supported by the European Commission, Grant EVG1-CT-1999-00011EFFS. We thank the MAP data centre (<http://www.map.ethz.ch>) for providing the high resolution precipitation data.

### References

1. The European Flood Forecast System (EFFS) project, <http://EFFS.wldelft.nl>
2. De Roo, A. P. J., J. Bartholmes, P. D. Bates, K. Beven, P. Bongioannini-Cerlini, B. Gouweleeuw, E. Heise, M. Hills, A. Hollingsworth, B. Holst, M. Horritt, N. Hunter, J. Kwadijk, F. Pappenburger, P. Reggiani, G. Rivin, K. Sattler, E. Sprokkereef, J. Thielen, E. Todini and M. Van Dijk, 2003: Development of a European Flood Forecasting System, *Journal of River Basin Management*, in press.
3. Steppeler, J., G. Doms, U. Schättler, H. W. Bitzer, A. Gassmann, U. Damrath, and G. Gregoric, 2003: Meso-gamma scale forecasts using the nonhydrostatic model LM. *Meteorology and Atmospheric Physics*, in press.
4. Majewski D., D. Liermann, P. Prohl, B. Ritter, M. Buchhold, Th. Hanisch, G. Paul, W. Wergen, and J. Baumgardner, 2003: The operational global icosahedral-hexagonal gridpoint model GME: description and high-resolution tests, *Monthly Weather Review*, **130(2)**, 319–338.

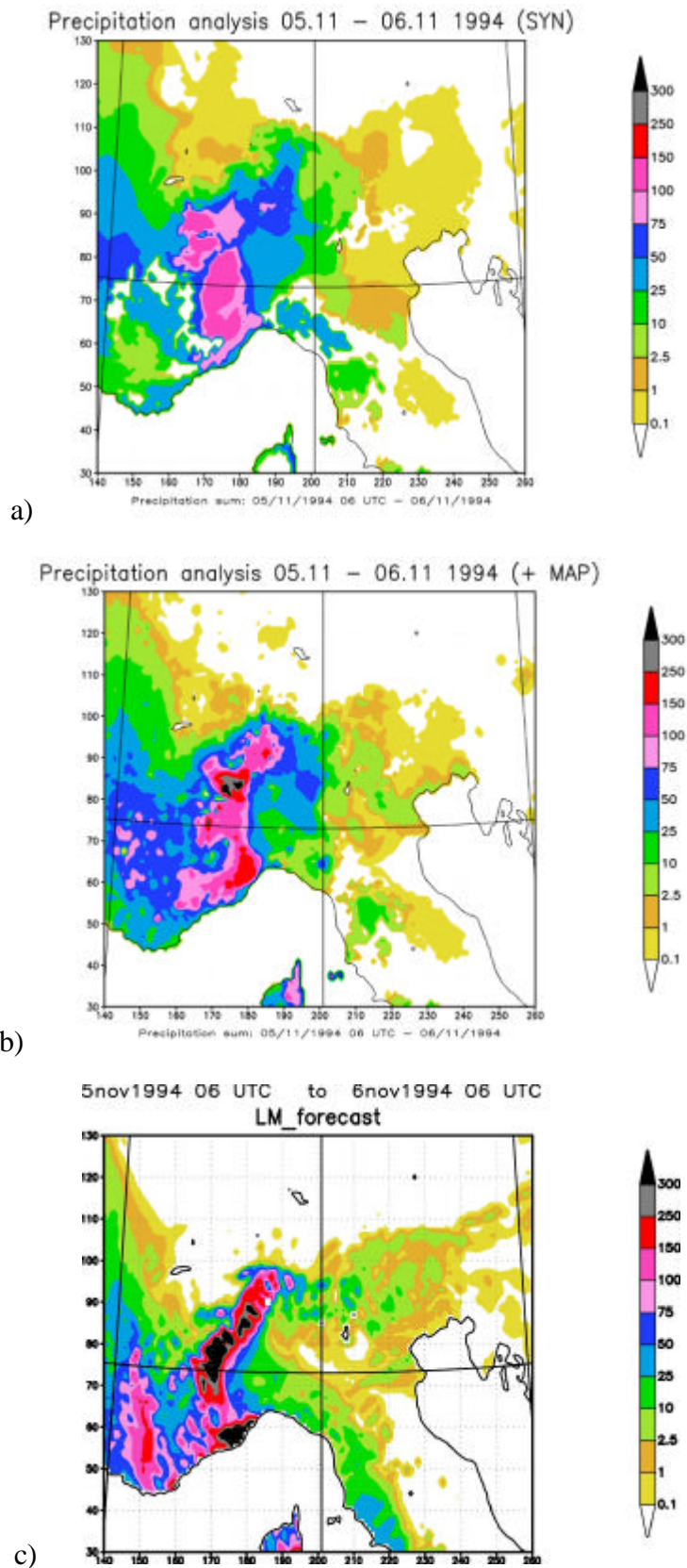


**Figure 1:** Precipitation distribution ( $\text{kg}/\text{m}^2$ ) for 05 Nov, 1994, 06 UTC to 06 Nov, 1994, 06 UTC. a) Analysis based on network of synoptic stations, b) analysis based on synoptic and MAP stations, c) model prediction. See text for details.

## GRIPS GCM simulated polar vortex intercomparison

Gregory L. Roff (Email: g.roff@bom.gov.au)

*Australian Bureau of Meteorology Research Centre  
150 Lonsdale St, Melbourne, Victoria, Australia 3000*

The 4D evolution of stratospheric polar vortex simulations within GRIPS GCM models (Pawson et al, 2000) are compared with analyses (NMC and UKMO) by applying elliptical diagnostics (Waugh, 1997) to daily output over several years. Details of the datasets used are seen in Table 1.

Elliptical diagnostics (Waugh, 1997) provide a concise method to depict the 4D lifecycle of stratospheric polar vortices and are obtained by fitting an ellipse to the Ertel potential vorticity (E<sub>pv</sub>) contour which defines the edge of the polar vortex on isentropic surfaces. The characteristics of the fitted ellipse (equivalent latitude, centroid latitude and longitude, aspect ratio and orientation of the major axis) are then used to describe the vortex.

Given the time series of daily geopotential height fields the E<sub>pv</sub> is calculated via Randel (1992). Because the magnitude of E<sub>pv</sub> increases rapidly with height we use the modified E<sub>pv</sub> of Lait (1994) and we define the vortex edge as the location of the highest E<sub>pv</sub> gradient with respect to the equivalent latitude of each E<sub>pv</sub> contour, constrained by the proximity of a strong westerly jet (Nash et al., 1996).

The time mean, maximum, minimum and standard deviation of the absolute equivalent latitude ( $|elat|$ ) for the southern hemisphere polar vortex for the analyses and model datasets are plotted in Figure 1. The NMC and UKMO analyses plots suggest that the polar vortex is: “S” shaped; centred near 60°; with a local  $|elat|$  maxima near 700K; a rapid increase in vortex size and variability above 1000K; and a local  $|elat|$  minima near 1500K with rapid decay of the vortex above.

Most of the model vortices tend to capture some of these main features but the shape of the vortex is greatly affected by model characteristics such as: horizontal and vertical resolution; the presence of sponge layers; gravity wave drag schemes; model top location; radiation schemes and planetary wave characteristics.

### References

Lait, L.R., 1994: J. Atmos. Sci., 51, 1754-1759.

Nash, E.R. et al., 1996: J. Geophys. Res., 101, 9471-9478.

Pawson S. et al., 2000: Bull. Amer. Met. Soc., 81, 4, 781-796.

Randel, W.J., 1992: NCAR Technical Note NCAR/TN-366+STR, February, 1992.

Waugh,D.W., 1997: vortices. Q.J.R. Meteorol. Soc., 123, 1725-1748.

Group	Contact	Horiz Resolution no. Lat X Lon	No. of Vert Levels	Top (hPa)	Time Span
NMC analyses, USA	W.Randel	40x36	L17	1.00	21 years
UKMO analyses, UK	BADC	72x96	L22	0.31	9 years
BMRC, Australia	G.Roff	72x144	L34	0.31	10 years
CMAM, Canada	J.de Grandpre	48x96	L50	0.01	10 years
CNRM, France	P.Simon	32x64	L31	0.03	20 years
FUB, Germany	U.Langematz	32x64	L27	0.01	20 years*
MPI, Germany	E.Manzini	64x128	L39	0.01	5 years*
MRI-JMA, Japan	K.Shibata	64x128	L24	0.01	15 months
NASA, USA	S.Pawson	91x144	L55	0.015	10 years
UM-UKMO, United Kingdom	R.Bannister	72x96	L58	0.10	20 years

Table 1: *The group, contact scientist, resolution and reference for the GRIPS GCM models and analyses used in this study. \* Note that FUB provided three different model runs and MPI two.*

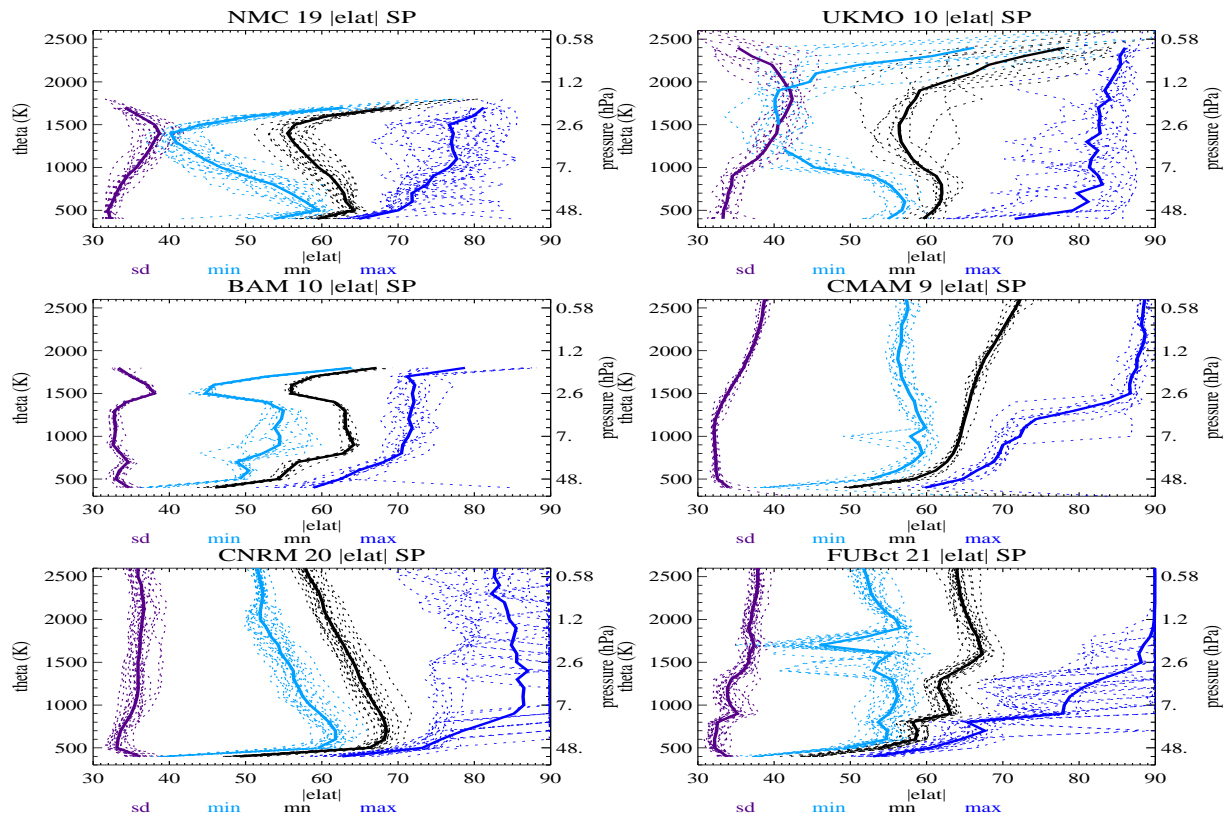
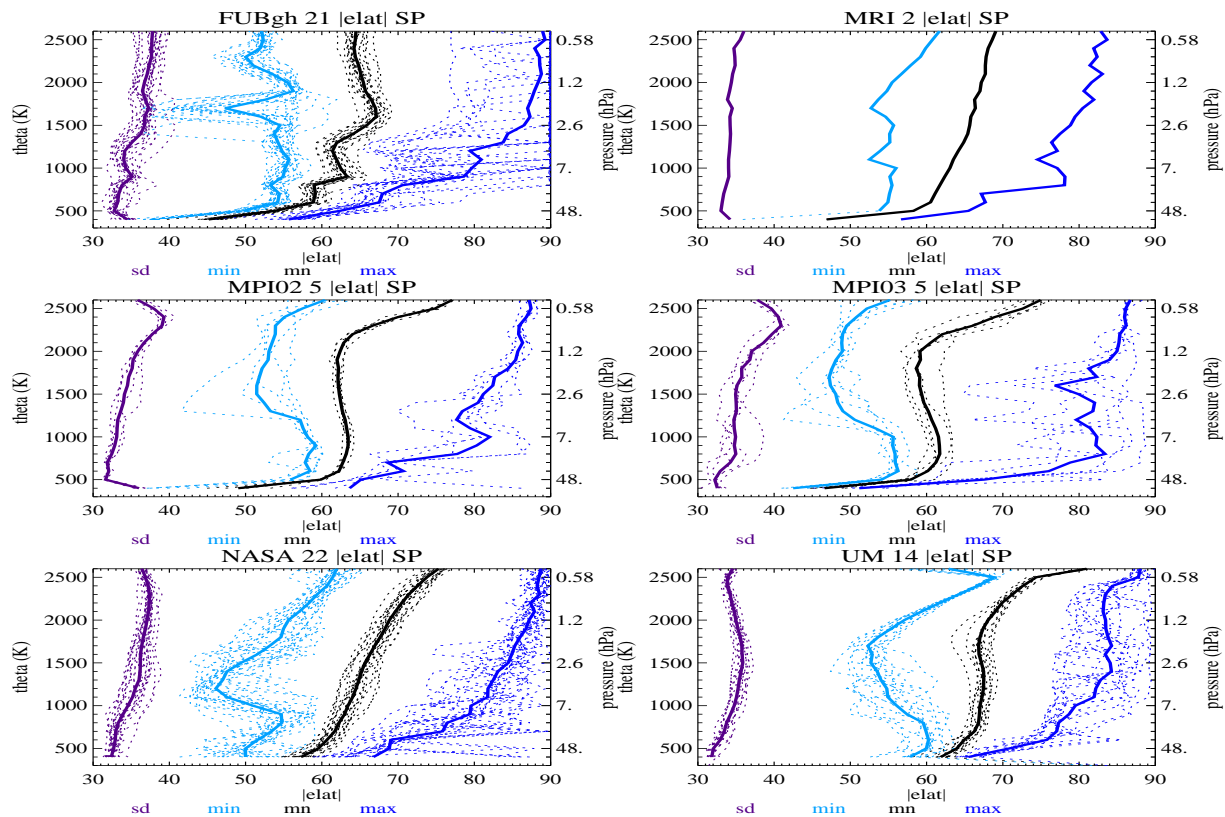


Figure 1: The mean, maximum, minimum and standard deviation (black, dark blue, light blue and purple curves, respectively) of the absolute equivalent latitude ( $^{\circ}$ ) for the southern hemisphere polar vortex calculated for daily data from each year (dashed curves) and averaged over all years (solid curves) for 2 analyses and 10 model datasets plotted against potential temperature (K).



## Tropical Cyclogenesis Detection in the East Pacific Hurricane Basin

Ryan J. Sharp, Mark A. Bourassa, and James J. O'Brien

Center for Ocean-Atmospheric Prediction Studies (COAPS), The Florida State University

The SeaWinds scatterometer provides high-resolution spatial coverage and temporal observations of vector winds over the global oceans. These data can be accessed in near-real-time (NRT) to provide another means of identifying areas that are favorable for tropical cyclogenesis (TCG). Liu (2001) and Katsaros et al. (2001) both used subjective analysis to identify when the closed circulation of the tropical cyclones (TCs) in the Atlantic could first be identified in the SeaWinds data. Sharp et al. (2002) used an objective method that specifically looked for a minimum vorticity derived from the SeaWinds data to identify potential areas of TCG in the Atlantic hurricane basin.

This report follows up on the work of Sharp et al. (2002) by reporting on the success of the method in identifying areas of TCG in the East Pacific hurricane basin during the 2001 and 2002 seasons. We apply the vorticity-based test to the NRT QuikSCAT data for these seasons. Of the over 2000 swaths through the domain during that period, the objective test identifies a total of 415 that contain potential tropical systems. Most of these systems are pre-existing TCs (e.g., Adolph of 2001 was identified in 11 separate swaths).

Almost all of the TCs (29 of the 33) from the two seasons have at least one swath identifying the TCG that occurred prior to their development into TCs. The average lead time for these systems is 36 hrs before they became TCs. The longest lead time for 2001 was for tropical depression 6 with a 79 hr lead time (Fig. 1A). The wind vectors not contaminated by rain indicate a broad closed circulation. However, thunderstorm activity was not persistent in the area of the circulation, so the system did not qualify as a TC. For 2002, Lowell had the longest lead time at 56 hrs (Fig 1B), and again

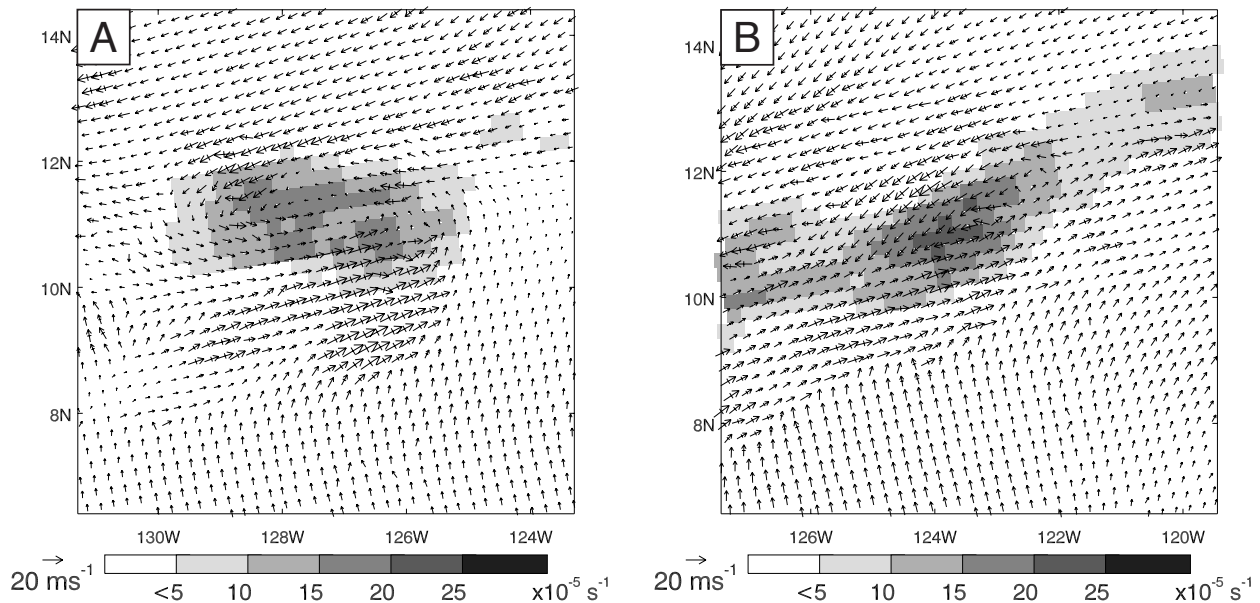


Fig. 1: SeaWinds wind and spatially averaged vorticity for T. D. 6 (A, 1419 UTC 19 August 2001) and Lowell (B, 1357 UTC 20 October 2002). The background shading represents vorticity, and the length of the arrows indicates the strength of the wind. Arrows with a bar through them indicate data that may be contaminated by rain.

persistent thunderstorm activity did not follow this system. The structure of the wind field also indicated more of a shear line as opposed to a definite closed circulation.

The objective technique has an excellent probability of detection (94.8%) when a TC is within a swath. The false alarm rate, the number of identified systems that never became a TC divided by the total number of identified systems, is 42.1%. Some of these false alarms were apparent closed surface circulations that never fully developed the characteristics of a TC. The critical success index, the number of 'good' identifications divided by the sum of the total number of identified systems plus the number of missed identifications, is 0.566.

The circulations identified by our objective method during TCG indicate that processes occurring at the surface must be important to TCG. Further work is underway to determine why certain systems develop and others do not.

### *Acknowledgments*

Gene Legg and Paul Chang at NOAA/NESDIS provided the NRT data used in this report. Thanks to Jiraporn Whalley and Stacey Campbell for their help in automating the retrieval and processing of that data. Thanks also to Jesse Enloe, Anthony Arguez, and Chance Haynie for their work with the beta operational project. NASA support was provided through funding for the Ocean Vector Wind Science Team. The National Oceanographic Partnership Program (NOPP) provided support for operational scatterometry. The Center for Ocean-Atmospheric Prediction Studies receives its base funding from the Office of Naval Research's Secretary of the Navy grant to James J. O'Brien.

### **References**

- Katsaros, K. B., E. B. Forde, P. Chang, and W. T. Liu, 2001: QuikSCAT's SeaWinds facilitates early identification of tropical depressions in 1999 hurricane season, *Geophys. Res. Lett.*, **28**, 1043-1046.
- Liu, W. T., 2001: Wind over troubled waters. *Backscatter*, **12**, 10-14.
- Sharp, R. J., M. A. Bourassa, J. J. O'Brien, 2002: Early detection of tropical cyclones using SeaWinds-derived vorticity, *Bull. Amer. Meteor. Soc.*, **83**, 879-889.

## Origins of northern Antarctic Peninsula air masses

Ian Simmonds  
School of Earth Sciences  
The University of Melbourne  
Victoria, Australia, 3010  
Email: simmonds@unimelb.edu.au

The Antarctic Peninsula (AP) has a number of characteristics which makes its weather and climate rather different from those of the rest of Antarctica. It is the most northerly part of the continent, and hence is the most subject to midlatitude influences and its north-south orientation influences transient weather systems in a variety of ways. The AP is of especial current interest because the rate at which the western side has warmed over recent decades (e.g., Doran et al., 2002) and also because it has experienced the disintegration over the last decade of a number of its ice shelves, including parts of the Larsen ice shelf. In February 2002 the northern section of the Larsen B shelf shattered and separated from the continent. A number of studies have quantified the roles of weather and climate in these breakups (e.g., Scambos et al., 2000).

The understanding of the atmospheric dynamics of this data-sparse part of the world has been aided by reanalysis products (e.g., Simmonds et al., 2003). We here make use of the NCEP/DOE reanalysis (Kanamitsu et al., 2002) available every 6 hrs over the period 1 January 1979 to 29 February 2000. The broad region to the west of the Peninsula is host to vigorous synoptic activity (Simmonds and Keay, 2000) and hence there is a rich variety of air trajectories which reach the AP. To quantify the variety of regional influences on the northern part of the Peninsula we have calculated the origin points of all 850 hPa four-day trajectories which reach 304.5°E, 63.1°S (near Esperanza on the northern tip of the AP) using the accurate technique described in Perrin and Simmonds (1995). The wide variety of origin points can best be conveyed by presenting their spatial frequency distribution. Fig. 1 shows that greatest frequency of summer (DJF) departure points is found some 40° to the west of Esperanza, as one might have expected. However, the distribution function is quite broad; significant numbers of trajectories start from more than 90° upstream of the AP, and a considerable proportion originate from the east. Many starting points are found as far north as 45°S over South America. A similar, if a little more diffuse, plot for winter (JJA) is displayed in Fig. 2. The greater spread reflects even more active and varied circulations in that season.

Doran, P. T., and Coauthors, 2002: Antarctic climate cooling and terrestrial ecosystem response. *Nature*, **415**, 517-520.

Kanamitsu, M., and Coauthors, 2002: NCEP-DOE AMIP-II Reanalysis (R-2). *Bull. Amer. Meteor. Soc.*, **83**, 1631-1643.

Perrin, G., and I. Simmonds, 1995: The origin and characteristics of cold air outbreaks over Melbourne. *Aust. Meteor. Mag.*, **44**, 41-59.

Scambos, T. A., and Coauthors, 2000: The link between climate warming and break-up of ice shelves in the Antarctic Peninsula. *J. Glaciol.*, **46**, 516-530.

Simmonds, I., and K. Keay, 2000: Mean Southern Hemisphere extratropical cyclone behavior in the 40-year NCEP-NCAR reanalysis. *J. Climate*, **13**, 873-885.

Simmonds, I., K. Keay and E.-P. Lim, 2003: Synoptic activity in the seas around Antarctica. *Mon. Wea. Rev.*, **131**, 272-288.

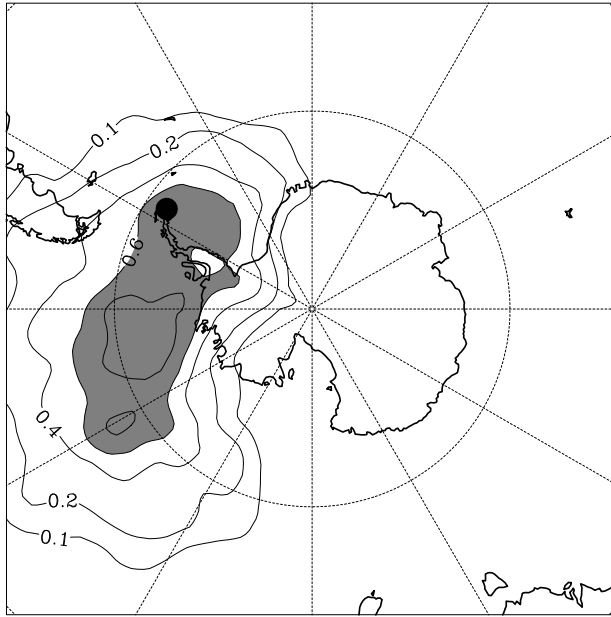


**Figure 1:** Frequency distribution of origin points of all summer (DJF) 4-day 850 hPa trajectories which terminate at  $63.1^{\circ}\text{S}$ ,  $304.5^{\circ}\text{E}$  (indicated by a solid dot). The contour interval is 0.2 origin points per 1000  $(\text{deg. lat.})^2$  per trajectory, and an extra contour has been added at 0.1.

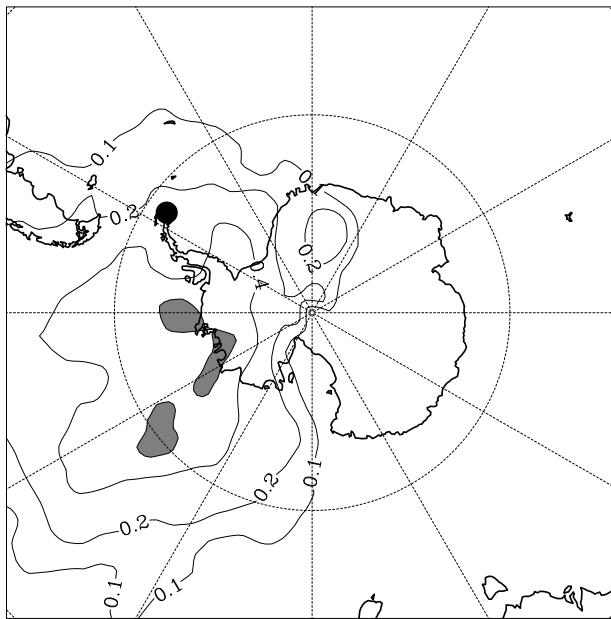


**Figure 2:** As Figure 1, but for winter (JJA).

## Tropical Pacific wind comparisons: objective FSU versus NCEP reanalysis products

Shawn R. Smith, Mark A. Bourassa, and Rosario Romero

Center for Ocean-Atmospheric Prediction Studies

The Florida State University, Tallahassee, FL, 32306-2840, USA

[smith@coaps.fsu.edu](mailto:smith@coaps.fsu.edu)

Global reanalysis projects at NCEP and ECMWF have provided the researchers investigating climate change and ocean-atmosphere modeling with uniformly assimilated data sets. The surface air-sea flux fields from reanalyses are now widely used to force models. Since air-sea fluxes play a critical role in ocean variability, quality estimates of these parameters are essential to numerical simulations of the ocean-atmosphere system. Comparing flux fields from reanalysis products to products derived from other data sources, and using different parameterizations, can provide estimates of the uncertainties in the reanalysis fields.

The Center for Ocean-Atmospheric Prediction Studies has developed and made operational a new objective procedure to create monthly mean turbulent flux fields over the ocean (Bourassa et al. 2001). The input data are all in-situ and include ships of opportunity and buoys (both moored and drifting). Buoy and ship observations are independently weighted and background fields are based on the observations. A variational method utilizes several constraints to maximize similarity to observations, minimize non-geophysical features in the spatial derivatives (e.g., the observational patterns), and accomplishes these goals with the minimum smoothing necessary. Weights are objectively determined using cross validation (Pegion et al. 2000).

Comparisons over the tropical Pacific Ocean are made between the objective FSU winds and the wind fields from the first and second NCEP reanalysis (NCEPR1 and NCEPR2 respectively). Monthly wind averages over the equatorial Pacific (11N - 11S, 122 - 290E) reveal large differences in the three products (Figure 1). When comparing long term means, the FSU winds are stronger ( $5.6 \text{ ms}^{-1}$ ) than either the NCEPR1 ( $4.1 \text{ ms}^{-1}$ ) or the NCEPR2 ( $4.6 \text{ ms}^{-1}$ ). The  $1.5 \text{ ms}^{-1}$  difference in means between FSU and NCEPR1 is consistent with Smith et al. (2001), in which they compared wind observations from research vessels (R/V) to the NCEPR1 and found the NCEPR1 winds in the tropics to be consistently lower (mean bias  $0.7 \text{ ms}^{-1}$ ) than the R/V winds. Since the R/V winds are rarely included in the NCEPR1 and are not used in the FSU products, they provide a pseudo-independent reference for the FSU and NCEP wind fields. The difference between the NCEPR2 and FSU is smaller ( $1.0 \text{ ms}^{-1}$ ) than for NCEPR1 and the reduction may be due to either improvements in the data inputs to NCEPR2 or changes in the NCEPR2 flux parameterization. The authors plan to investigate the differences between the NCEPR1 and NCEPR2 parameterizations to determine what role they play in reducing the NCEP versus FSU differences.

In contrast to the monthly wind averages, the monthly standard deviation in the equatorial Pacific wind speeds are similar for the FSU and NCEP reanalyses. Long term mean standard

deviations are  $0.59 \text{ ms}^{-1}$  for the FSU product and  $0.54 \text{ ms}^{-1}$  for both the NCEPR1 and NCEPR2. This implies that all three products capture a similar level of monthly wind variability, while the mean winds differ greatly for each product.

These results, though preliminary in nature, imply that improvements in near surface winds have been made in NCEPR2 for the tropical Pacific. The authors analysis will continue and will be expanded to include momentum and heat fluxes in the near future.

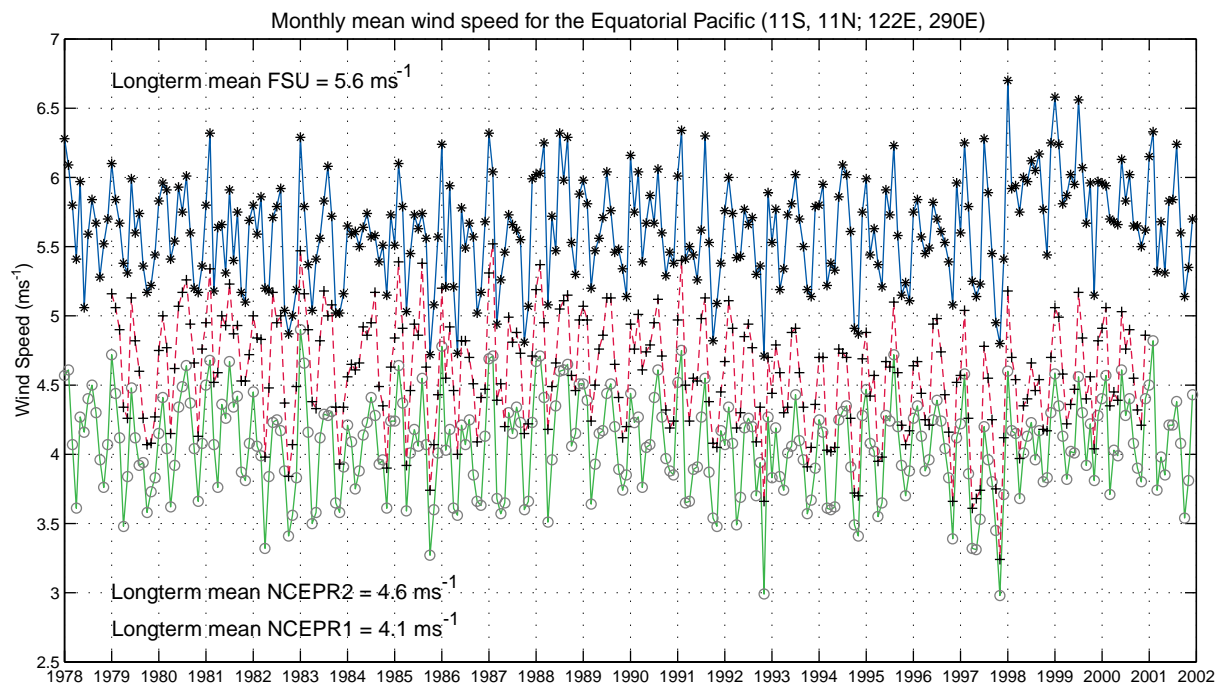


Figure 1: Monthly mean wind speed ( $\text{ms}^{-1}$ ) averaged over the Equatorial Pacific from  $11^{\circ}\text{S}$  to  $11^{\circ}\text{N}$ ,  $122$  to  $290^{\circ}\text{E}$  for the objective FSU (\*, blue solid line), NCEP Reanalysis 1 (O, green solid line), and NCEP Reanalysis 2 (+, red dashed line).

*Acknowledgments.* Support provided by NSF Ocean Sciences and the NOAA Office of Global Programs.

Bourassa, M. A., S. R. Smith, and J. J. O'Brien, 2001: A new FSU winds and flux climatology. *11<sup>th</sup> Conference on Interactions of the Sea and Atmosphere*, San Diego, CA, Amer. Meteor. Soc., 9-12.

Pegion, P. J., M. A. Bourassa, D. M. Legler, and J. J. O'Brien, 2000: Objectively-derived daily "winds" from satellite scatterometer data. *Mon. Wea. Rev.*, **128**, 3150-3168.

Smith, S. R., D. M. Legler, and K. V. Verzone, 2001: Quantifying uncertainties in NCEP reanalyses using high-quality research vessel observations. *J. Climate*, **14**, 4062-4072.